Chapter 5

Reconfigurable On-board Power Processor with Wired and Wireless Charging for Electric Vehicle

5.1 Introduction

Wireless charging of Electric Vehicle (EV) is an alternative to traditional wired charging method, which offers hassle-free charging experience to the customer with a futuristic approach. Facilitating this additional advance feature in an EV requires an additional on-board power-processing unit (PPU) to be included in the vehicle. The addition of an extra unit in the vehicle increases the cost, weight and volume of the vehicle. The additional weight of this PPU reduces the vehicle efficiency in terms of miles on a single charge, as this unit is to be carried by the vehicle throughout its journey.

In an EV, the propulsion unit is the prime power module that keeps it moving. This module includes a propulsion motor and a power electronic interface, which converts DC to three phase AC for driving the motor. In addition to this, separate power electronic modules are used for on-board wired and wireless charging systems. Thus, three PPUs are required for three modes of operations as shown in Fig. 5.1.

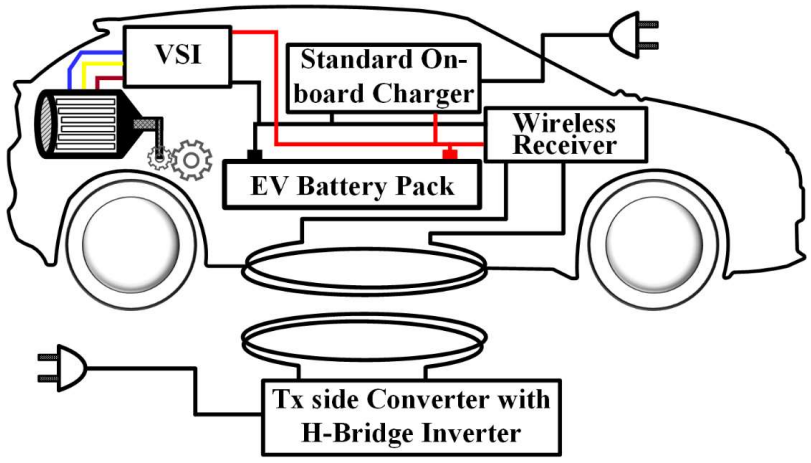

Fig. 5.1. Conventional architecture with wireless charging for electric vehicle.

In order to amalgamate these three power modules, this chapter proposes a reconfigurable power processor (RPP) for EV, capable of serving the purpose of three different power modules required for propulsion, wired charging and wireless charging as shown in Fig. 5.2. This optimizes the weight, volume and cost of the EV as separate power modules are avoided in three different modes of operation. In both the wired and wireless charging methods, the proposed technique draws power from the single-phase wall outlet and charges the EV battery pack using constant current-constant voltage (CC-CV) logic and performs power factor correction (PFC) operation at the input AC side. A laboratory scale prototype is developed for experimentally validating the proposed concept with a 24 V, 30 Ah battery set and a 24 V, 400 W BLDC motor.

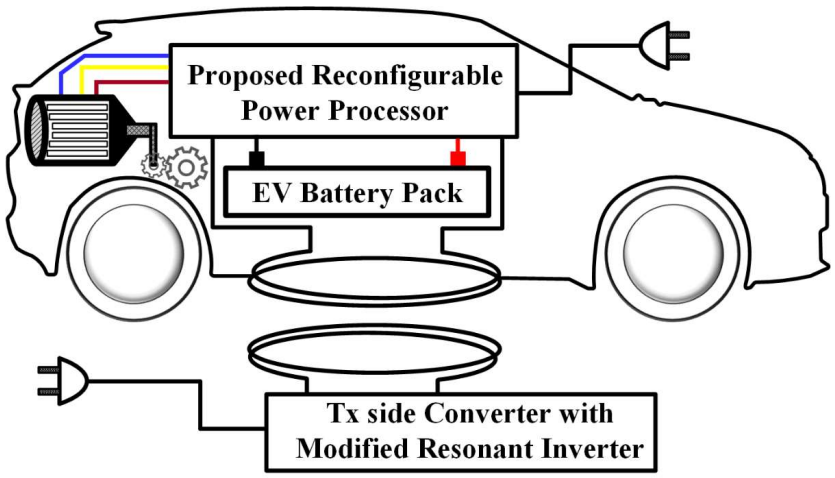

Fig. 5.2. System representation of the proposed work.

5.2 Derivation of the Topology

Propulsion unit is the most important power-processing unit in an EV as this unit converts DC power from the battery and drive the motor unit. So, the circuit topologies required for wired and wireless charging modes are derived from a three-phase voltage source inverter (VSI), which is commonly used as a propulsion unit in EV. The VSI consists of six power electronic switches in three legs (three half-bridges), which are reutilized to derive the required circuit topologies during both wired and wireless charging modes. The additional passive elements (L and C) are also considered in this case, to derive the required circuit as shown in Fig. 5.3.

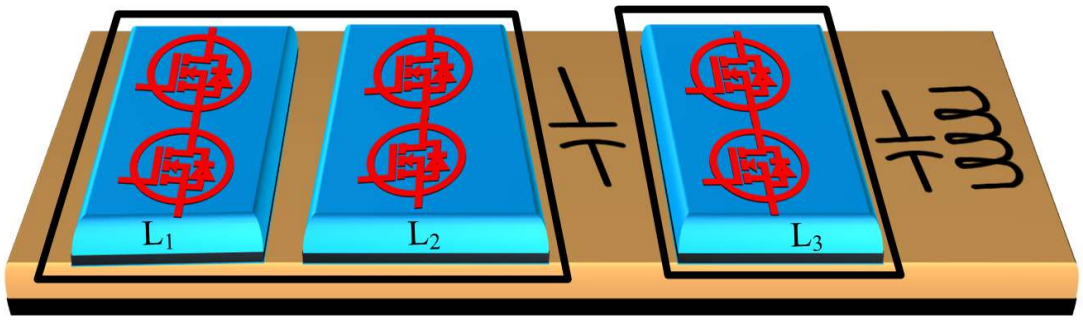

Fig. 5.3. Basic backbone of the proposed RPP

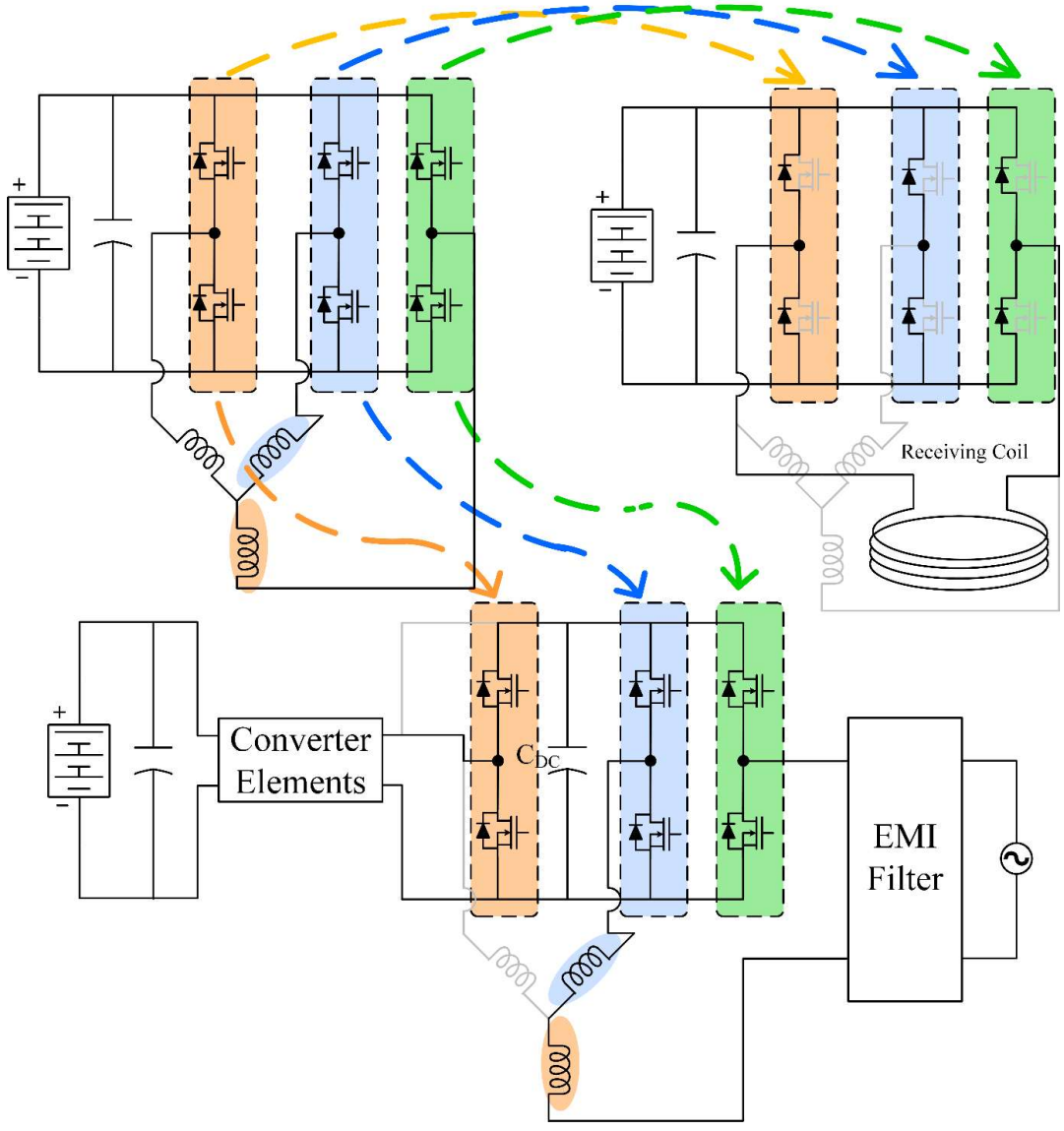

Fig. 5.4. Derivation of the wired charger and wireless receiver from the propulsion unit.

5.2.1 Derivation of Wired Charger

The first two legs of the three-phase VSI is reutilized as the AC-DC boost PFC stage, which acts as the stage-I of the wired charging system. The third leg is used as a half-bridge switching circuit, which produces square wave that varies between zero and the input DC-link voltage. Additionally, the motor windings are also reutilized as boost inductor at the input of stage-I of the wired charging topology as shown in Fig. 5.4.

5.2.2 Derivation of Wireless Receiver

The PPU at the receiving end converts high frequency AC from the receiving coil to DC for charging the EV battery pack. For this, an additional diode bridge rectifier is required at the vehicle end, which can be derived from the existing three-phase VSI as shown in Fig. 5.4.

Deriving multiple topologies from a single power-processing unit by reutilizing the components is possible by using suitable contactors, which has already been as discussed in chapter 3. For achieving three different modes out of a single power processor, a four-point contactor is required with one fixed contact and three moving contacts. The complete circuit schematic of the proposed RPP is shown in Fig. 5.5.

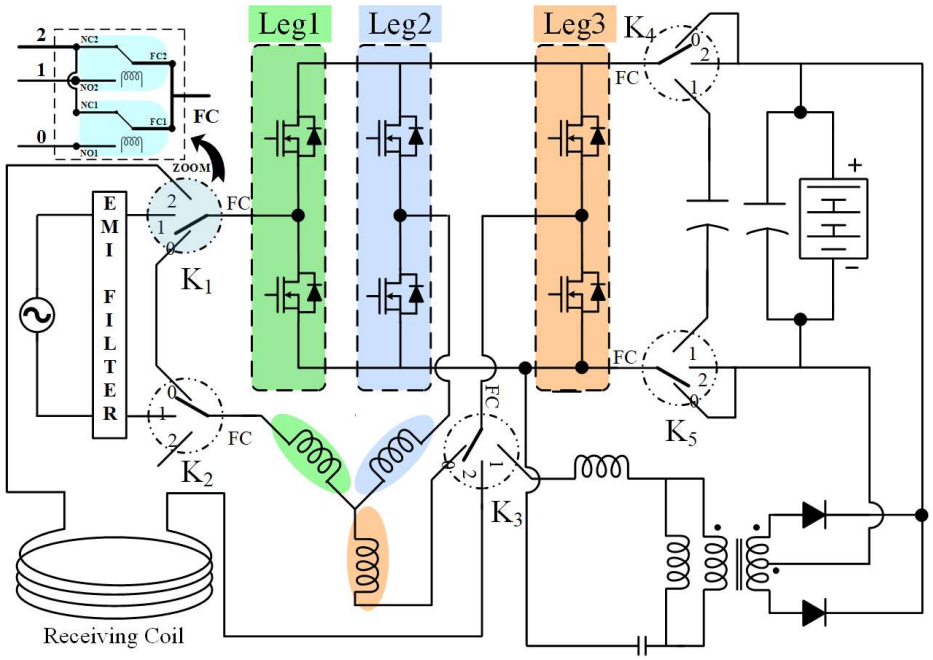

Fig. 5.5. The Proposed Reconfigurable Power Processor.

5.3 Operation and Control of the Proposed RPP in Different Modes

The proposed reconfigurable power processor is operated as three different topologies during three different modes of operations, which are propulsion mode, wired charging mode and wireless charging mode. Operational details of all three modes with corresponding control schemes are discussed as separate subsections in this section.

5.3.1 Propulsion Mode

5.3.1.1 Operation During Propulsion Mode

The proposed multimode power processor during propulsion mode is shown in Fig. 5.6. During this mode, the proposed RPP behaves as a three-phase VSI that draws power from the EV battery pack and converts it into three phase AC for driving the motor. All the contactors are in their position “0”, which is the NC (normally closed) position of the contactor. The fixed contact of the contactor is always connected to its NC position without energizing any of the electromagnetic coils of the contactor. Therefore, the NC position is assigned to propulsion mode to reduce the continuous power loss across the energizing coils of the actuating contactors, as the vehicle remains in propulsion mode for a longer duration as compared to both the charging modes.

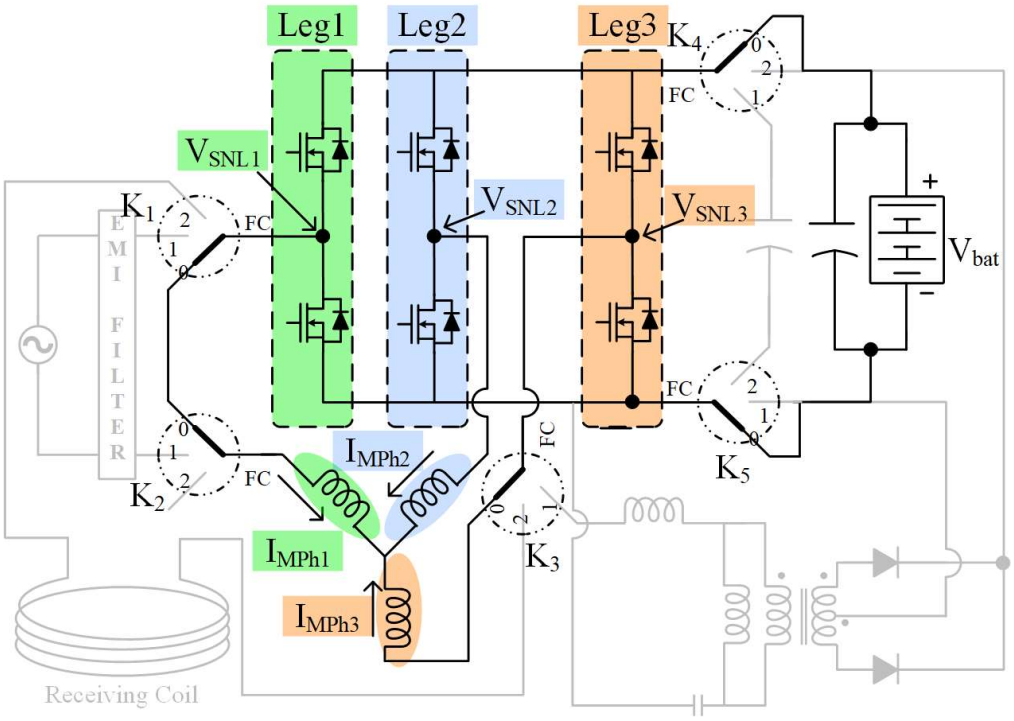

Fig. 5.6. Proposed power processor in propulsion mode.

Additionally, it is clear from the Fig. 5.6 that the diodes on the secondary side of the LLC circuit are reverse biased, and thus blocks the battery voltage to discharge through the LLC circuit. This reduces the need of additional contactors to isolate the battery pack from the wired charger circuit during this mode.

5.3.1.2 Control Scheme for Propulsion Mode

In order to drive the propulsion motor, control logic to run the BLDC motor is implemented in the chapter. The BLDC motor contains three inbuilt hall-effect sensors, positioned at a distance of 120° from each other. These arrangements result in a 60° resolution with six possible combinations of hall sensors output (zones) making a complete one rotation of 360°. The switching pattern for the VSI is decided depending upon the position of the flux density wave, which is a combined function of hall-effect sensors output. The switching patterns of all six switches for six different zones are given in Table 5.1.

Table 5.1. Switching States of the Proposed RPP during Propulsion Mode

Zone	Hall effect Outputs			Switching States during Propulsion Mode					
	PH_1	PH_2	PH_3	S_1	S_2	S_3	S_4	S_5	S_6
I	1	1	0	0	1	1	0	0	0
II	0	1	0	0	1	0	0	1	0
III	0	1	1	0	0	0	1	1	0
IV	0	0	1	1	0	0	1	0	0
V	1	0	1	1	0	0	0	0	1
VI	1	0	0	0	0	1	0	0	1

5.3.2 Wired Charging Mode

5.3.2.1 Operation During Wired Charging Mode

During the wired charging mode, all the contactors are set to their corresponding "position 1" to derive a standard two-stage on-board charger as shown in Fig. 5.7. The contactors K_1 and K_2 disconnect the motor phase windings and reconnect the mid-points of leg-1 and leg-2 to the input AC supply through an EMI filter. The motor windings PH_1 and PH_2 in series form the boost inductor (L_{boost}) at the input AC side. The Leg-1 and leg-2 in combination with the boost inductor form the stage-I of the charger. This stage is responsible for converting single-phase AC to a regulated DC supply with boost capability. The contactor K_3 connects the LLC circuit to the output of the half-bridge configuration to form the second stage of the on-board battery charger. The contactors K_4 and K_5 disconnect the battery pack from the three-legged structure and reconnect the output of stage-I to the DC-link capacitor. It can be noticed that both the stages of the charger are cascaded through this DC-link capacitor. Though the stage- I consists of four MOSFETs, only lower side MOSFETs are utilized as active switches and the body diodes of two higher side MOSFETs are used as part of active circuit in this mode. The simplified circuit diagram derived from the proposed RPP during wired charging mode is shown in Fig. 5.8.

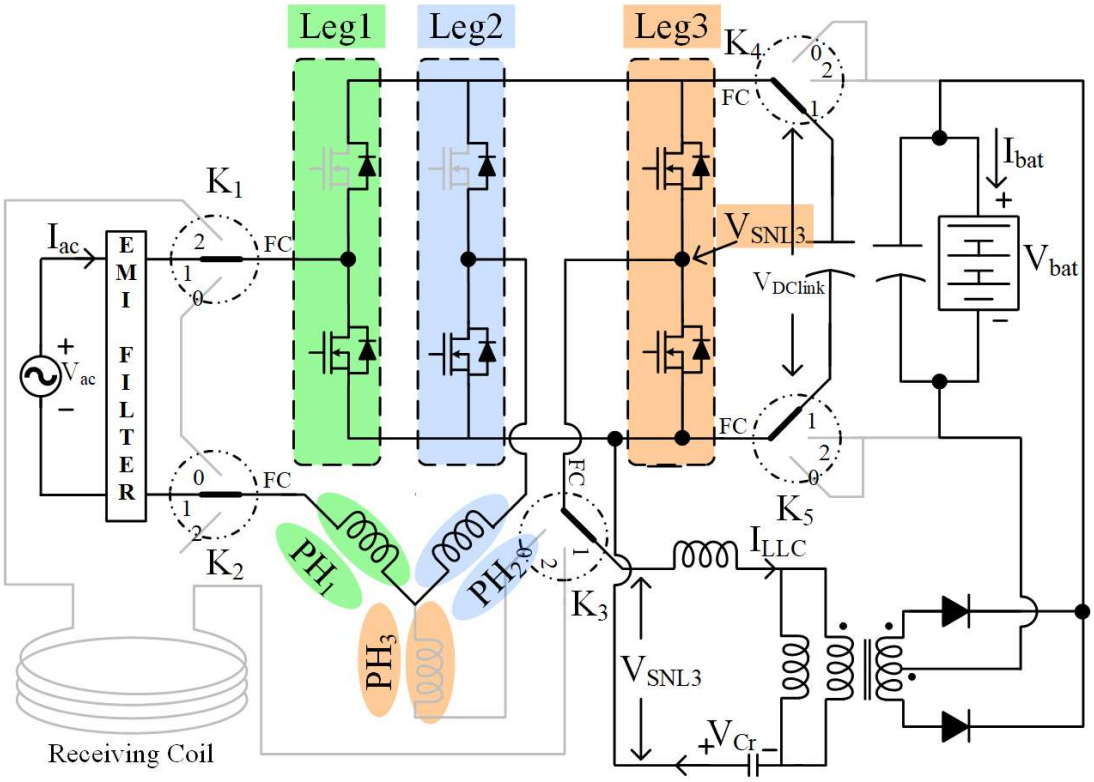

Fig. 5.7. Proposed power processor in wired charging mode.

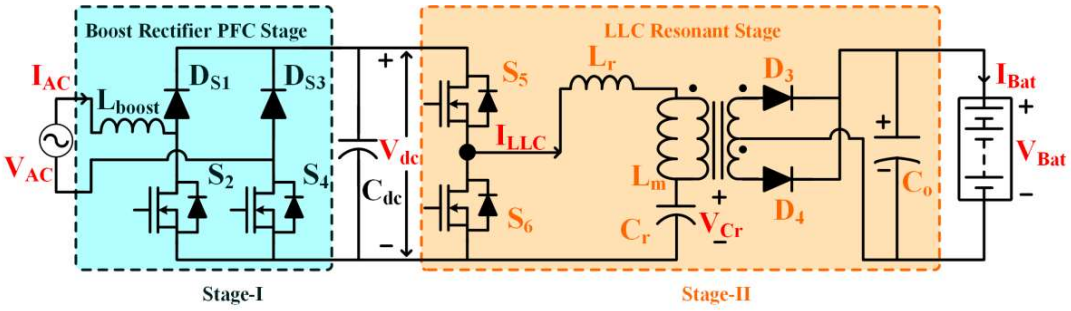

Fig. 5.8. Simplified circuit schematic of the on-board charger during wired charging mode.

It is evident from Fig. 5.8 that the stage-I of the charger operates as an AC-DC boost converter with PFC operation at the input side. During the positive half-cycle of the input AC supply, the switch S_2 along with the body diodes of switch S_1 (D_{S1}) and S_4 (D_{S4}) are ON. During the negative half-cycle, switch S_4 and body diodes of switch S_3 (D_{S3}) and S_2 (D_{S2}) are forward biased. Two lower side switches S_2 and S_4 conduct during two complementary half-cycles of the input AC supply and thus can be triggered using the same PWM signal.

The MOSFETs S_5 and S_6 are switched to produce a square wave voltage at the input of the LLC resonant tank, which then produces a sinusoidal output. This sinusoidal wave is then transferred to the secondary side using a high frequency transformer that provides galvanic isolation to restrict the supply side fault from appearing to the EV battery pack. The secondary side of this high frequency transformer uses a centre tapped full-wave rectifier configuration for converting high frequency AC to DC and optimally charging the battery.

5.3.2.2 *Control Scheme for Wired Charging Mode*

The complete control scheme during wired charging mode is presented in Fig. 5.9. The power stages and power lines are shown in red colour, while the signal lines and signal processing units are shown in black colour. The AC-DC front-end plant (first stage of wired charging mode) is operated with the controlled PWM, whereas the DC-DC converter (second stage of wired charging mode) is operated with a fixed duty at a constant frequency.

The battery terminals parameters (V_{bat} and I_{bat}) are sensed continuously but I_{bat} is compared with the reference current signal during CC mode and V_{bat} is compared with the reference voltage level during CV mode. These reference current and voltage levels are decided by the CC-CV logic block as shown in Fig. 5.9. The sensed parameter from the battery terminals is first divided by the gain of the second stage as the second stage is operated as a constant gain stage (discussed in chapter 2). The signal is then divided by the corresponding sensor gain and compared with the reference signal and the error is fed to the proportional integral (PI) controller for maintaining constant current or constant voltage at the battery terminals. Additionally, power factor improvement is taken care by the PFC controller, where the reference signal is the input voltage so that the input current drawn from the grid should follow the input AC voltage. To incorporate the effect of both PI and PFC controllers, both the controllers are cascaded by multiplying the output of PI to the input sensed voltage as shown in Fig. 5.9. Finally, the output of this cascaded system is used for generating the PWM signal that is used to feed the stage-I of the wired charger.

The switching pattern for stage-I of the charger generated by this control scheme is presented in Fig. 5.10. It can be observed from Fig. 5.10 that the similar PWM signals are required for switches S_2 and S_4 during two complementary time periods. Therefore, the same PWM signal can be fed continuously to both the switches and the complete charger is controlled by a single controlled PWM.

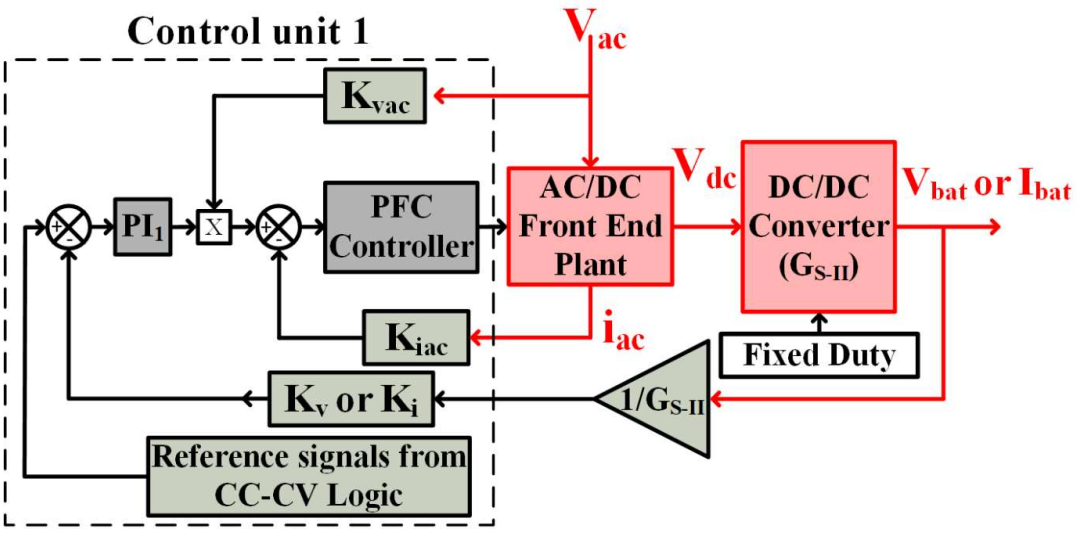

Fig. 5.9. Control scheme for the RPP during wired charging mode.

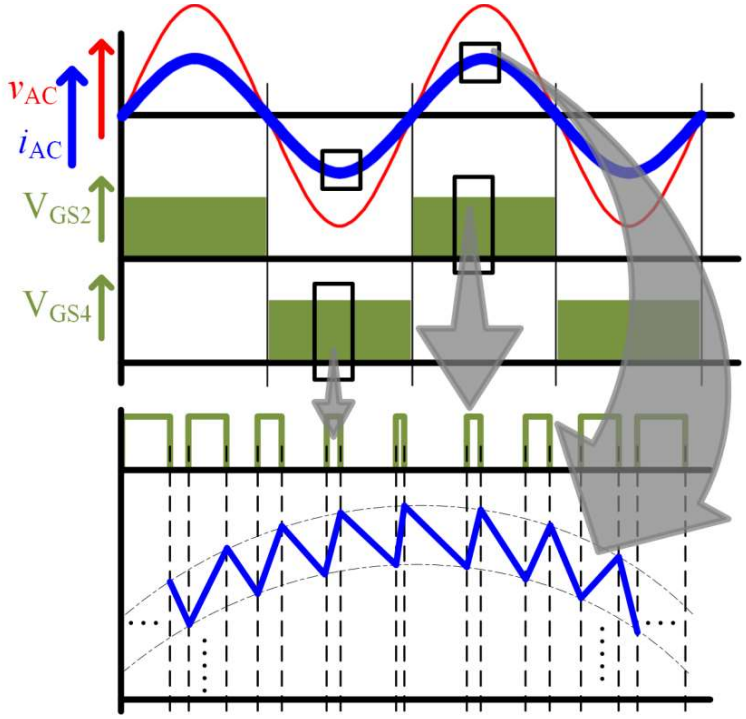

Fig. 5.10. Switching pattern for stage-I of the wired charging mode.

5.3.3 Wireless Charging Mode

5.3.3.1 Operation During Wired Charging Mode

In wireless charging mode, the proposed RPP serves the purpose of a receiving side converter as shown in Fig. 5.11. The received high frequency AC from the receiving side coil is converted to DC for charging the EV battery pack. All the contactors are set to their corresponding "position 2" for wireless charging mode. The contactors K_1 and K_3 connect the receiving side coils to the AC-DC rectifier and the contactors K_4 and K_5 connect the DC rail to the battery pack. The contactor K_2 has no role in this mode and thus its energizing coils can be left deactivated. In case of wireless charging, the only additional component added to the vehicle is the receiving coil, as the proposed RPP restructures itself to behave as the receiving side converter and thus saves additional cost and weight.

The transmitting side converter consists of an AC-DC front-end converter and an EF_2 inverter to generate high frequency AC waves for transferring power wirelessly. The detailed analysis and design criteria are already discussed in chapter 4. The compete schematics of the power electronic converters during wireless charging mode is presented in Fig. 5.12.

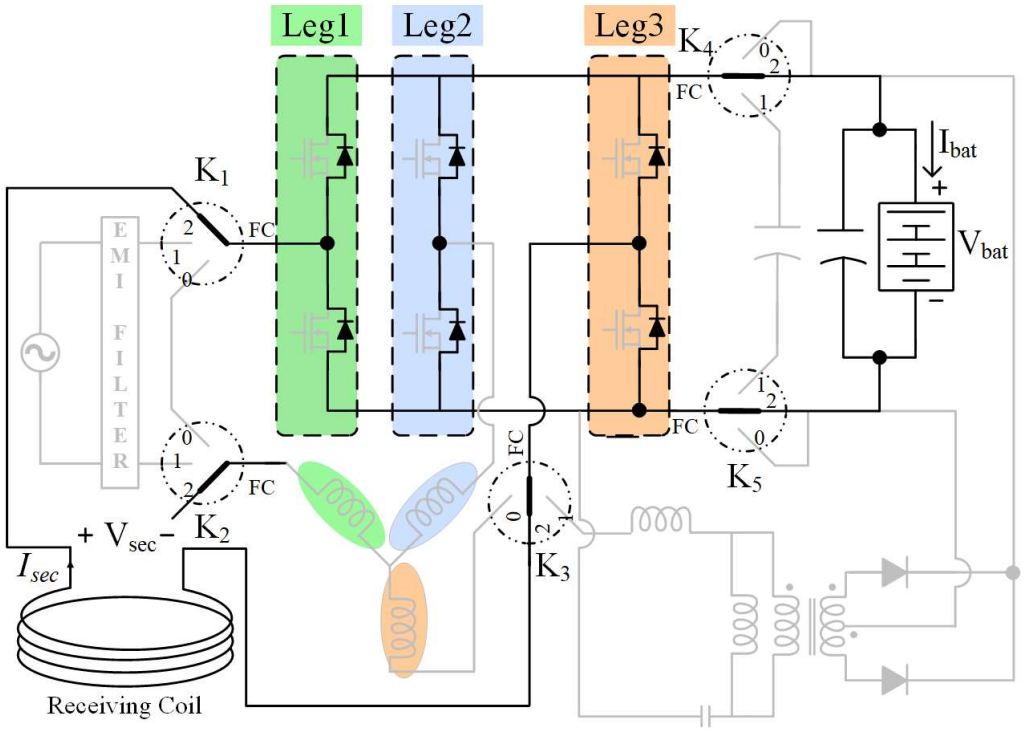

Fig. 5.11. Proposed power processor in wireless charging mode.

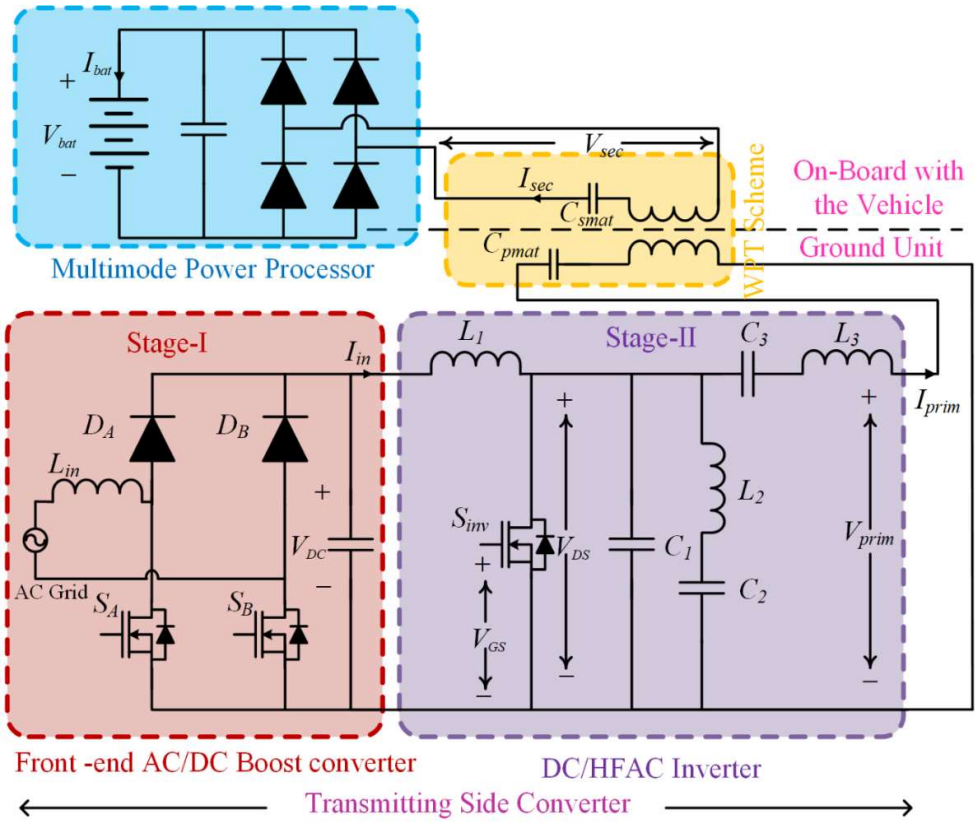

Fig. 5.12. Complete circuit diagram during wireless charging.

5.3.3.2 Control Scheme for Wireless Charging Mode

The complete control scheme for the proposed wireless charger is implemented using a TMS320F28335 DSP experimenters' kit as shown in Fig. 5.13. It can be observed that the battery terminal current and voltage are sensed continuously and compared with the corresponding reference signals depending upon the CC-CV algorithm to generate the error signal V_{er1}. The PI controller processes this error signal and generates the required control signal. The obtained control signal is multiplied to the grid side AC voltage and then compared with the input current to generate V_{er2}. The PFC controller processes this error to generate the final control signal that drives the switches S_A and S_B of the AC/DC boost converter. The stage-II of the transmitting side converter is operated with a fixed duty ratio at resonant frequency and does not require any controller. Thus, only by controlling switches S_A and S_B, both CC-CV at the battery side and PFC at the grid side are achieved.

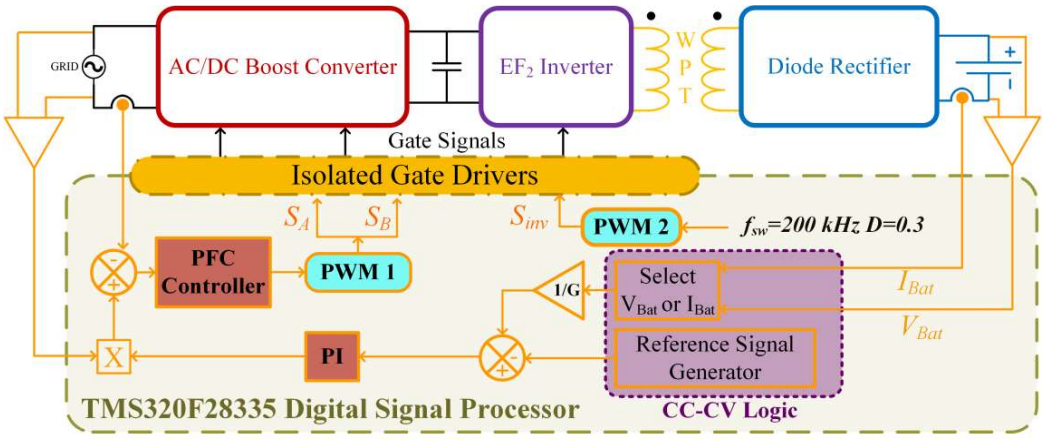

Fig. 5.13. Control scheme of the proposed topology during wireless charging mode.

5.4 Realization of a Four-Point Contactor

Three different circuit topologies during three different modes are achieved by using electromechanical contactors (relays). To restructure the proposed reconfigurable power processor into three different modes, the system requires four-point contactors, where one fixed contact can be connected to any of the available three moving contacts as shown in Fig. 5.14 (a). During the experimental stage, no other suitable contactors with proper rating could be found that has a single pole triple throw configuration as shown in Fig. 5.14 (a). In order to realize a four-point contactor, two numbers of three-point contactors are combined and connected in a unique fashion as shown in Fig. 5.14 (b). This combination is used as a four-point contactor. The two coils of the three-point contactors are designated as EC_1 and EC_2. The energizing coils EC_1 and EC_2 are turned ON according to the selected modes.

In a complete charging and discharging cycle of an EV, the vehicle operates in the propulsion mode for a longer duration as compared to wired or wireless charging modes. So, the NC positions of both the relays are shorted to operate in propulsion mode (mode 0) in order to minimize the losses across the coils of the relays. This has an additional advantage of carrying more current as the power rating during propulsion mode is higher than the charging modes. Thus, without operating any contactor coils, propulsion mode is achieved from the proposed RPP. This saves power losses in the coils and offers higher current carrying capability of the power processor. The coil EC_1 of all the relays are energized to achieve wired charging mode (mode 1), whereas coil EC_2 of all the contactors are energized to achieve wireless charging mode (mode 2).

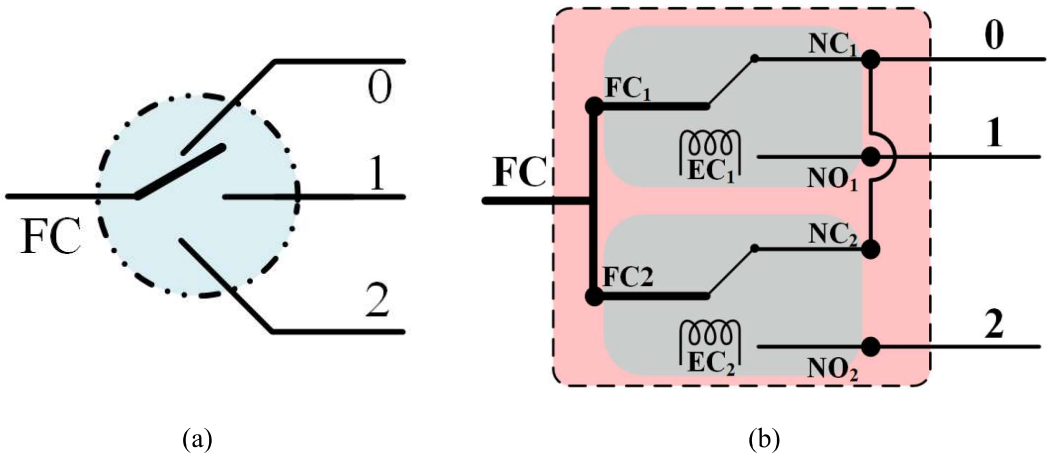

Fig. 5.14. Single pole triple throw switch, (b) Realization of a SPTT using two SPDTs.

5.5 Experimental Verification

The proposed algorithm is validated experimentally using 24 V, 30 Ah battery set and 400 W BLDC motor. The per-phase inductance and resistance of the motor are 150 µH and 100 mΩ respectively. The photograph of the complete experimental setup is shown in Fig. 5.15. The photograph of the proposed RPP showing all the interface ports is shown in Fig. 5.16.

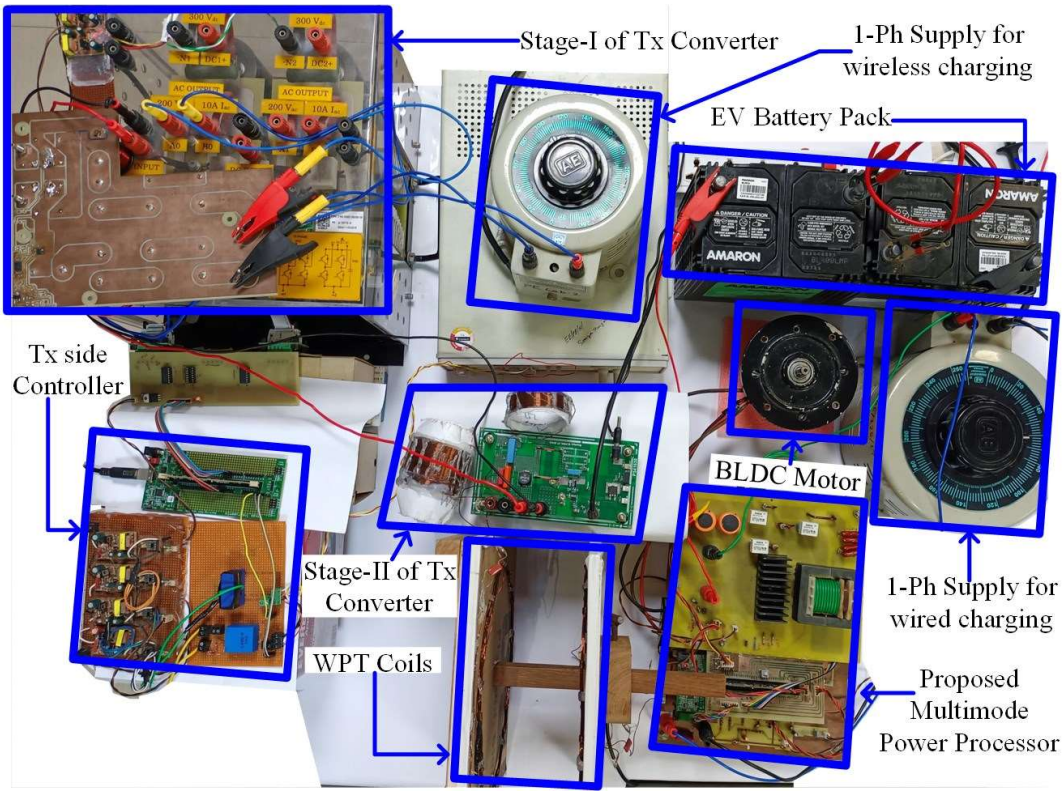

Fig. 5.15. Photograph of the complete experimental set-up including transmitting unit.

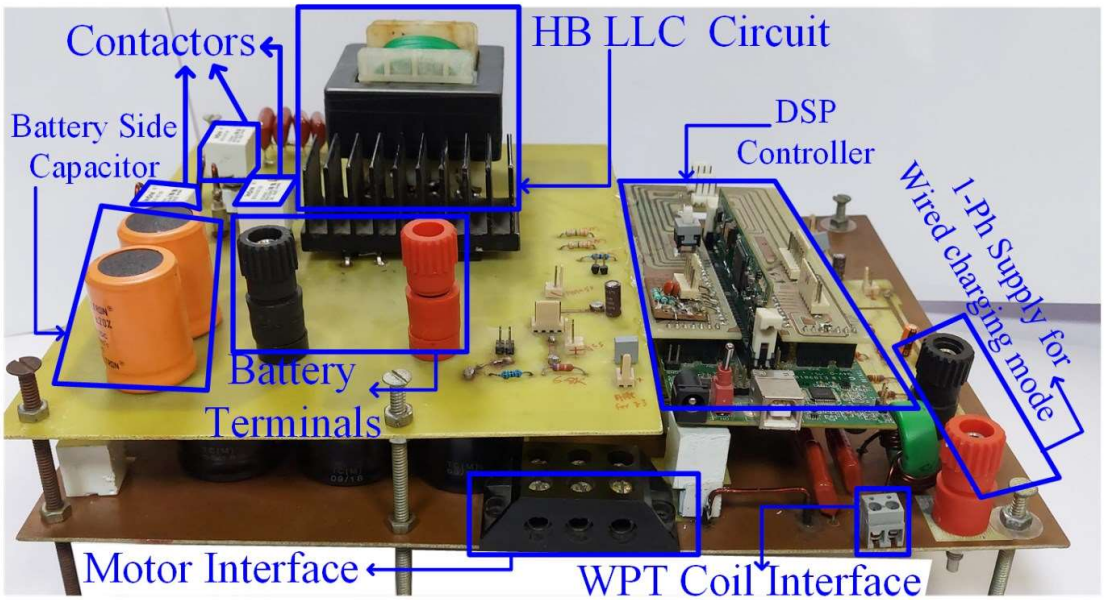

Fig. 5.16. Photograph of the proposed reconfigurable power processor.

5.5.1 Validation of Propulsion Mode

A 24 V, 400 W BLDC motor is tested using the proposed converter in the motoring mode. In this mode, the power flows from the battery pack to drive the motor through the inverter part of the proposed converter. The node voltage of all three nodes of the inverter is shown in Fig. 5.17 along with the battery voltage (V_0). The motor winding current of all the three phases are shown in Fig. 5.18. From both the Fig. 5.17 and Fig. 5.18, it is clear that the input voltage at the BLDC motor terminals and the current through the windings are 120° apart from each other.

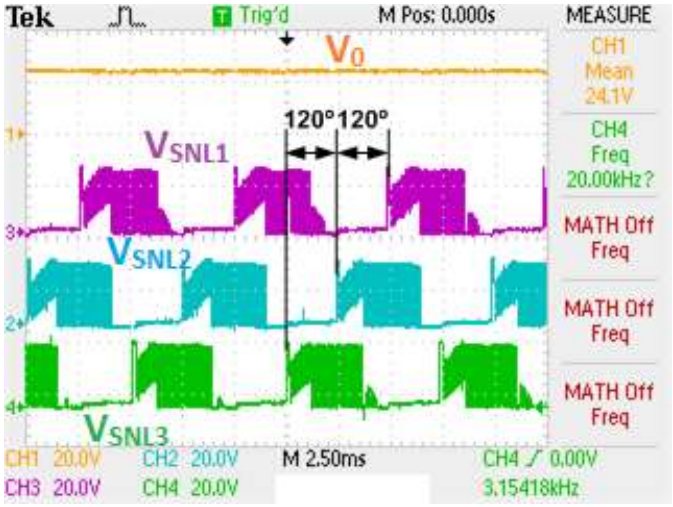

Fig. 5.17. Switch node voltages of the RPP with battery voltage for propulsion mode.

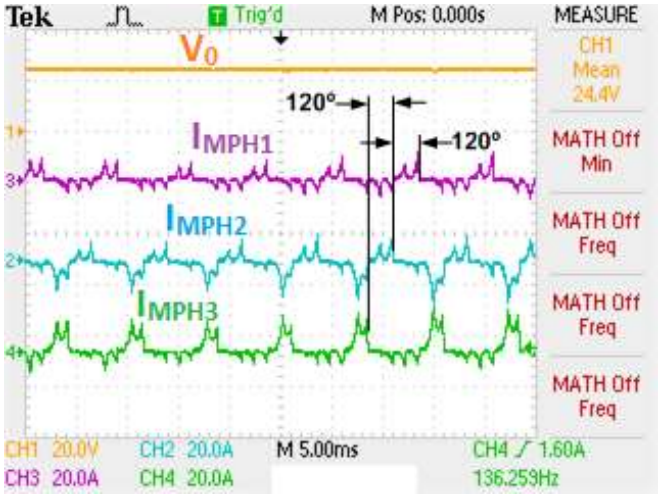

Fig. 5.18. Phase currents of BLDC Motor with battery terminal voltage during propulsion mode.

5.5.2 Validation of Wired Charging Mode

5.5.2.1 Testing of the Prototype

The proposed power processor forms a two-stage standard on-board charger with galvanic isolation during wired charging mode. The two-stage charger is tested for 24 V and 48 V battery sets. The Fig. 5.19 shows the operation of the charger for a 48 V battery with a constant current of 10 A, when the input voltage is 110 V AC (RMS). The Fig. 5.19 also confirms the PFC operation and results into near unity power factor. The Fig. 5.20 shows the operation of the second stage of the wired charging mode. In this mode, the DC link is switched using a half-bridge and then it is fed to the LLC resonant circuit to produce a sinusoidal current (I_{LLC}) at the primary side of the transformer. The current through the LLC tank (I_{LLC}) lags the tank input voltage (V_{SNL3}), which confirms zero voltage switching (ZVS) operation. The terminal voltage and current of the 24 V battery with grid side voltage and current during battery charging operation are shown in Fig. 5.21, which also confirms the PFC operation.

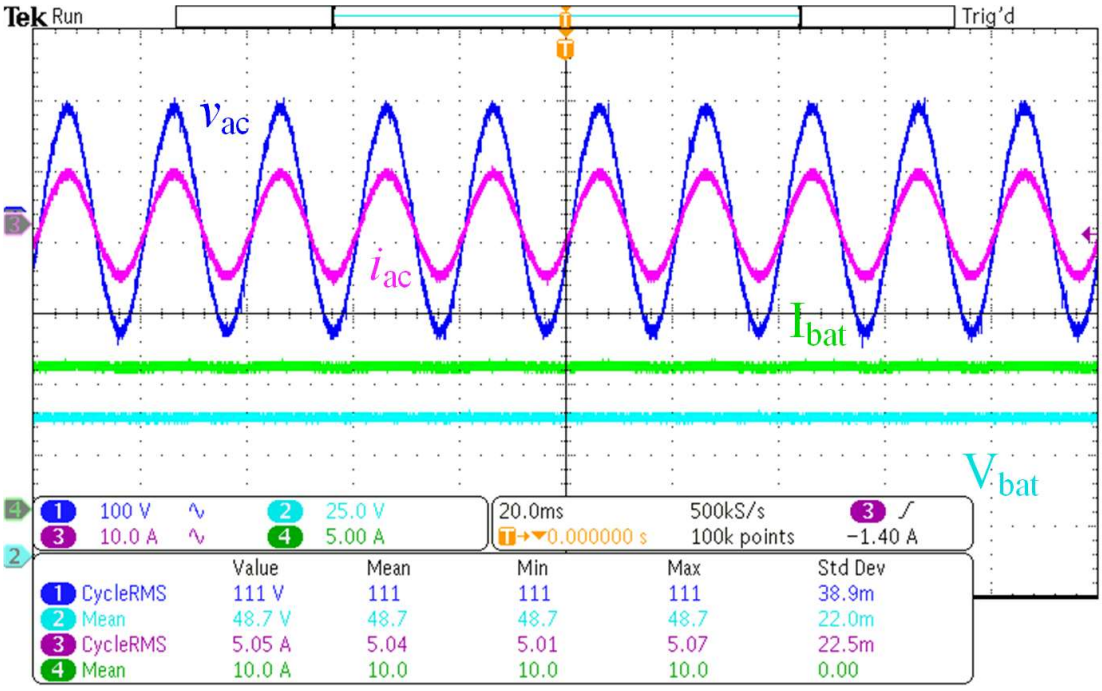

Fig. 5.19. Testing of wired charging mode with 48 V battery pack.

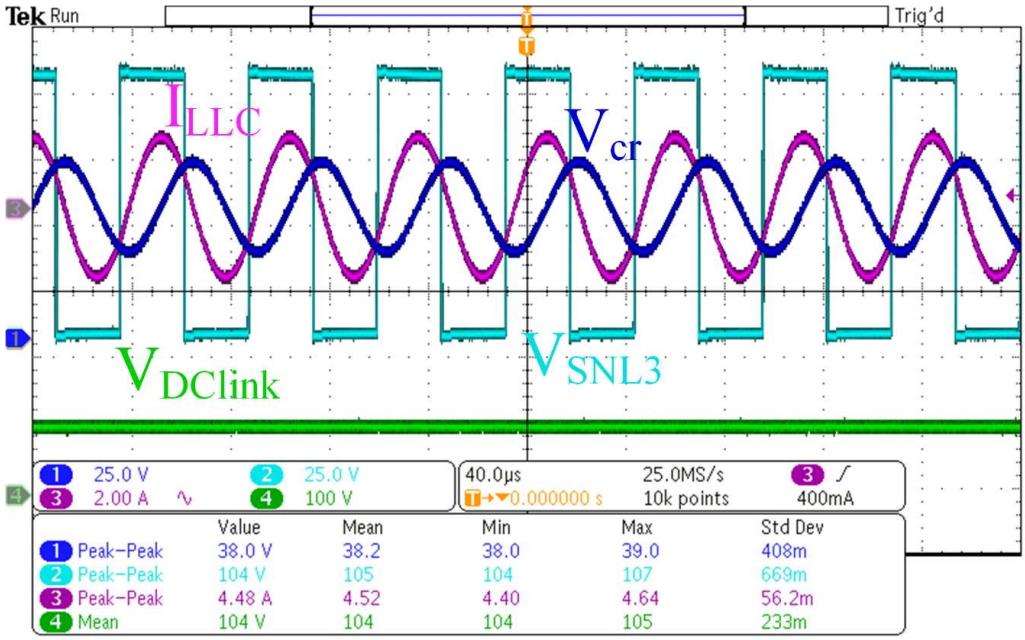

Fig. 5.20. Operation of stage- II during wired charging mode.

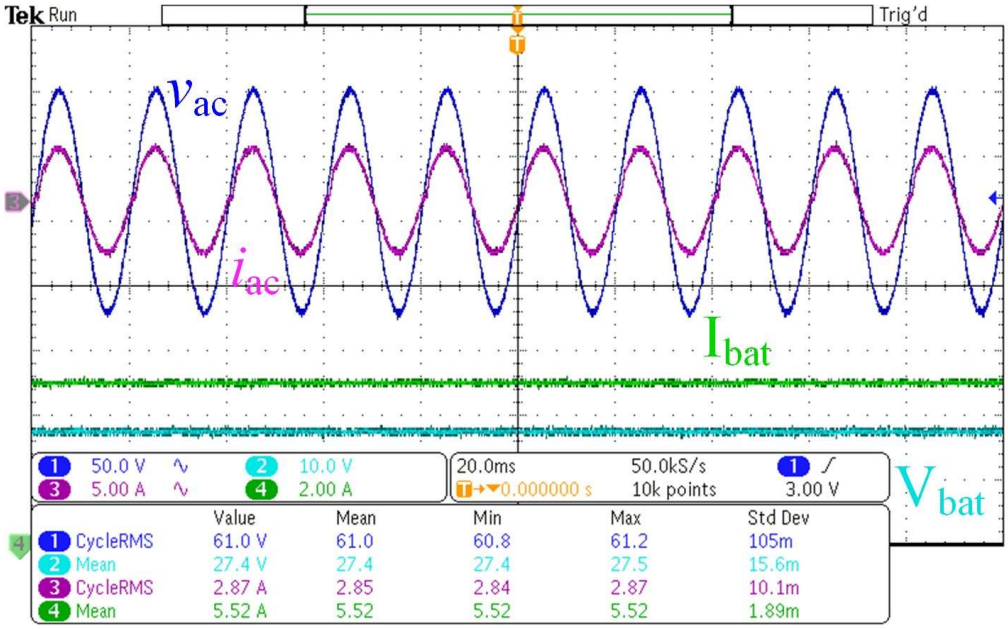

Fig. 5.21. Charging a 24 V, 30 Ah battery pack in wired charging mode.

The efficiency is also measured during this mode and was found to be dependent on the input AC voltage. The graph of efficiency versus battery terminal voltage at different AC input voltages are shown in Fig. 5.22. It is evident from the graph that the proposed power processor yields better efficiency at higher input AC voltage. However, this is limited by the test setup design and the maximum efficiency was found to be 97.6% when the input voltage is 70 V (RMS). The CC-CV curve achieved during charging of a 24 V, 30 Ah battery set is provided in Fig. 5.23.

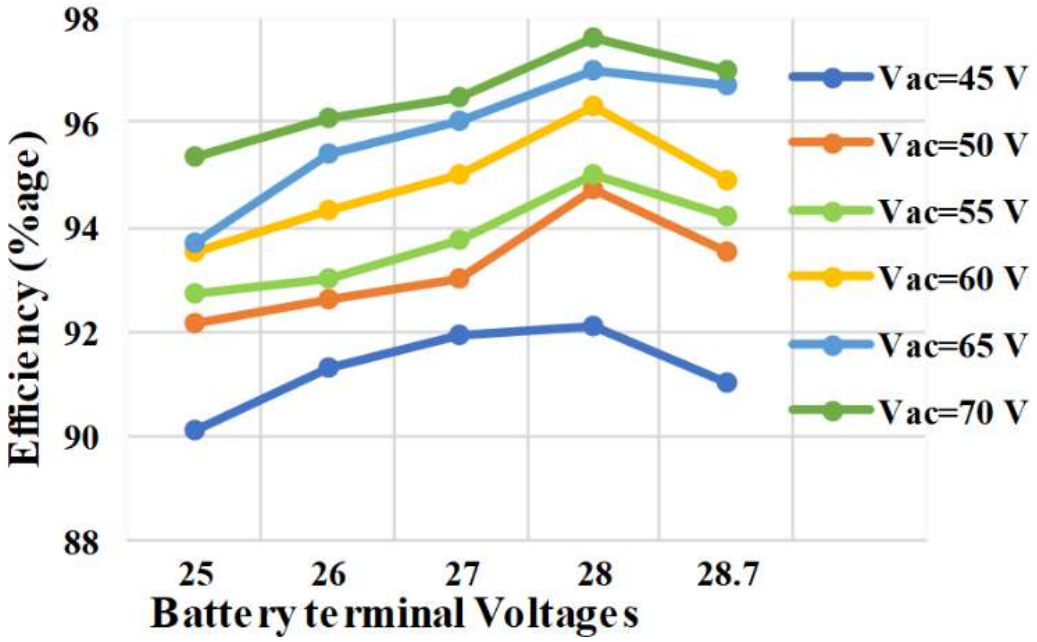

Fig. 5.22. Efficiency of the proposed power processor during wired charging mode.

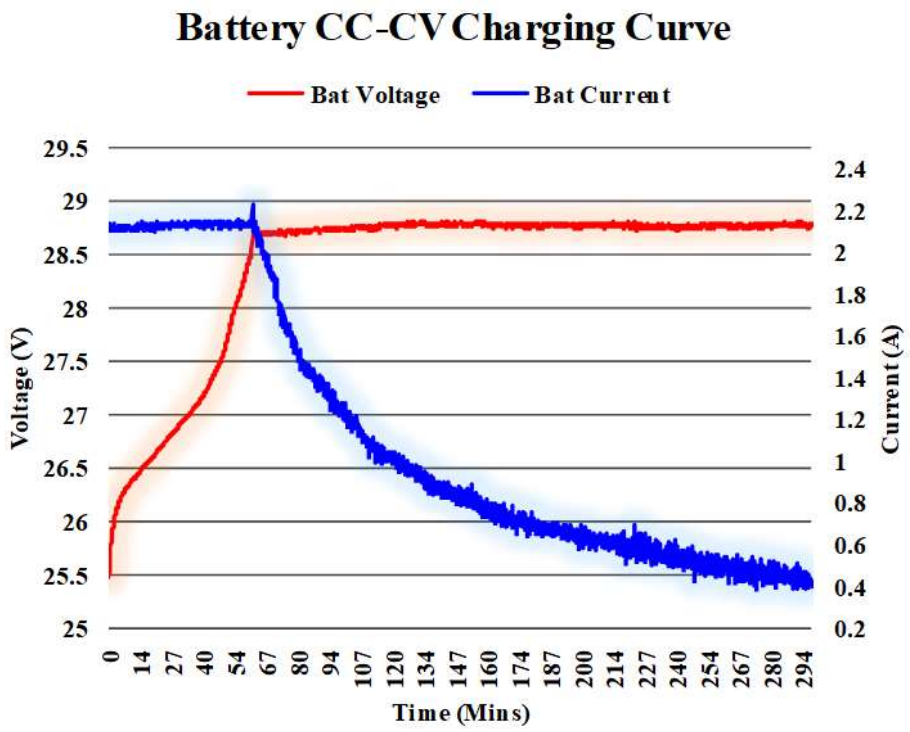

Fig. 5.23. CC-CV charging profile of the 24 V 30Ah battery set.

5.5.2.2 Power Loss Analysis and Distribution

During the positive half-cycle of input AC supply, switch S_2 (refer Fig. 5.8) is operated at a high frequency, which leads to switching losses across S_2 during the transition period. During the positive half-cycle, current flows through the S_2 and body diodes of S_4 (D_{S4}), when S_2 remain ON and the current flows through the body diode of S_1 and S_4 (D_{S1} and D_{S4}), when S_2 remains OFF. The conduction losses are calculated for the conducting switches and diodes. Similarly, the losses across various passive components are also determined and the loss distribution is calculated during the wired charging mode. The total loss is found to be 19.5 W, while delivering a power of 470 W with 96% efficiency. The loss distribution across various components (switching devices and passive elements) are calculated during this mode and are presented as percentage of total loss in Table 5.2. The same data are presented as bar chart in Fig. 5.24.

Table 5.2. Power Loss Distribution in Various Components of RPP during Wired Charging Mode

Components	Percentage loss	
	A	B
S_2, S_4	5.1% (Conduction Losses)	12.8% (Sw. Losses)
D_{S1}, D_{S3}	15.4% (Conduction Losses)	--
S_5, S_6	5.15% (Conduction Losses)	0 W
D_3, D_4	12.9% (Conduction Losses)	--
Boost Inductor	12.8% (Core Losses)	5.1% (Cu-Losses)
Transformer	15.35% (Core Losses)	10.25% (Cu-Losses)
All caps	5.15% (Total losses)	--

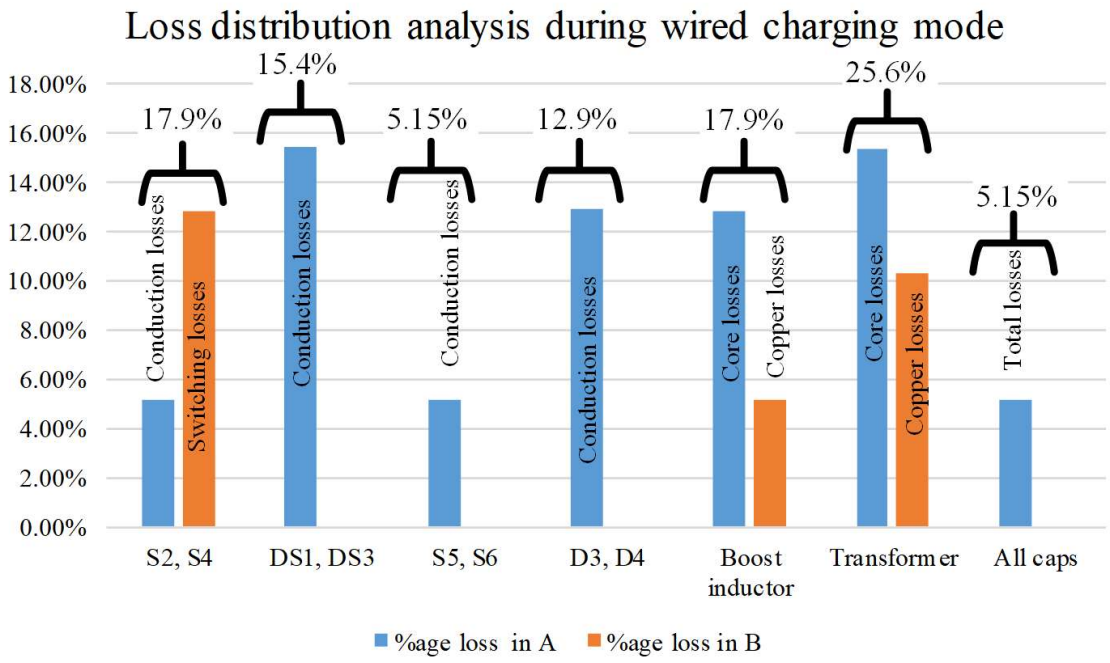

Fig. 5.24. Loss distribution in various components during wired charging mode.

5.5.3 Validation of Wireless Charging Mode

5.5.3.1 Testing of the Prototype

The proposed RPP forms a diode bridge rectifier during wireless charging mode, which acts as the receiving side power processor. In this mode, the forward voltage drop of the body diode of the MOSFET is found to be 1.5 V. The entire WPT scheme using the transmitting side power electronic module is tested in the laboratory environment for nearly up to 200 W. The EF_2 inverter is first tested with a resistive load for demonstrating ZVS operation. The output voltage, output current and the voltage stress across the inverter switch (S_{inv}) is shown in Fig. 5.25 with respect to the gate signal of the EF_2 inverter. The complete schematic as shown in Fig. 5.12 is tested using the proposed RPP for charging a 24 V battery wirelessly for a distance of 12 cm. The primary side voltage and current along with output voltage and current during the charging is shown in Fig. 5.26. The primary side voltage and current along with its secondary side counterparts are shown in Fig. 5.27. All the waveforms shown in Fig. 5.27 are sinusoidal and confirms the WPT operation. A 24 V battery set is charged wirelessly using the proposed scheme and the experimental results are shown in Fig. 5.28.

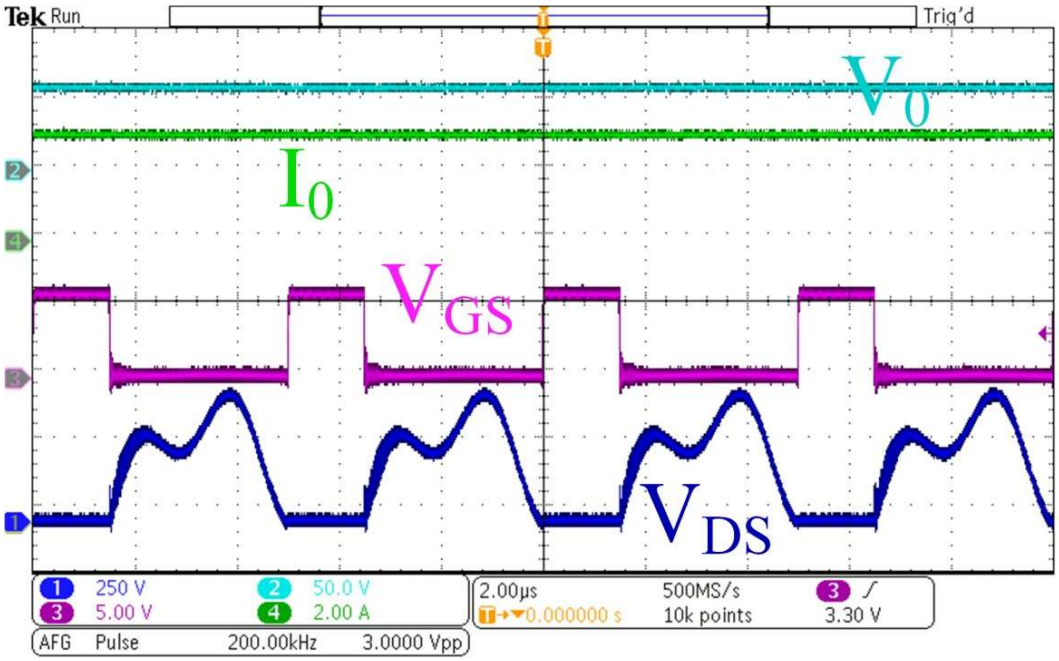

Fig. 5.25. Testing of EF_2 inverter demonstrating ZVS operation.

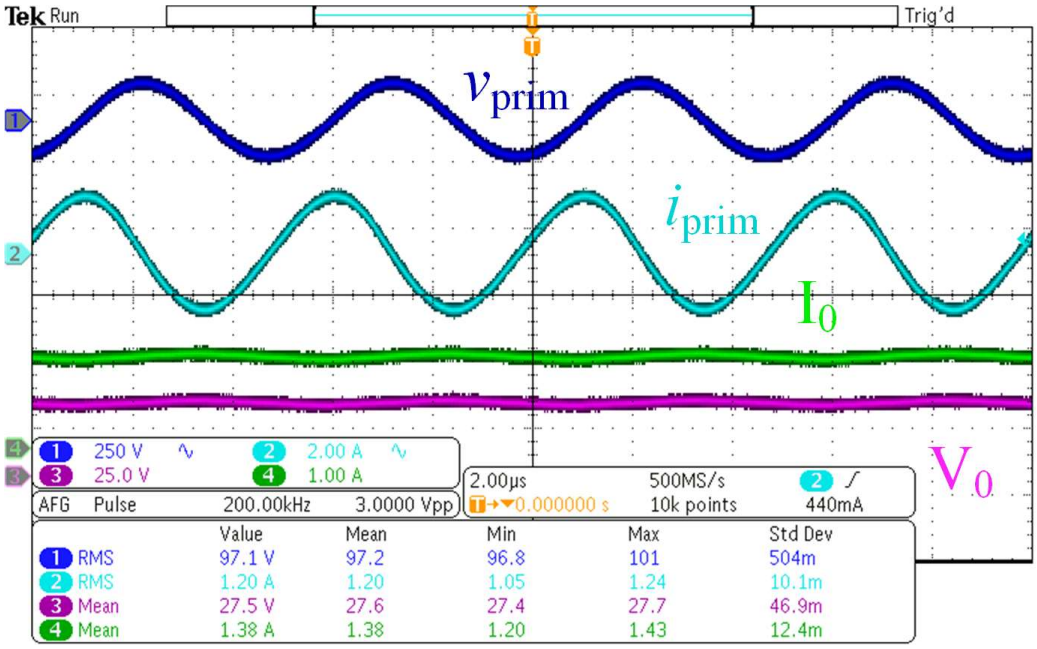

Fig. 5.26. Primary side voltage and current waveforms while charging the battery wirelessly.

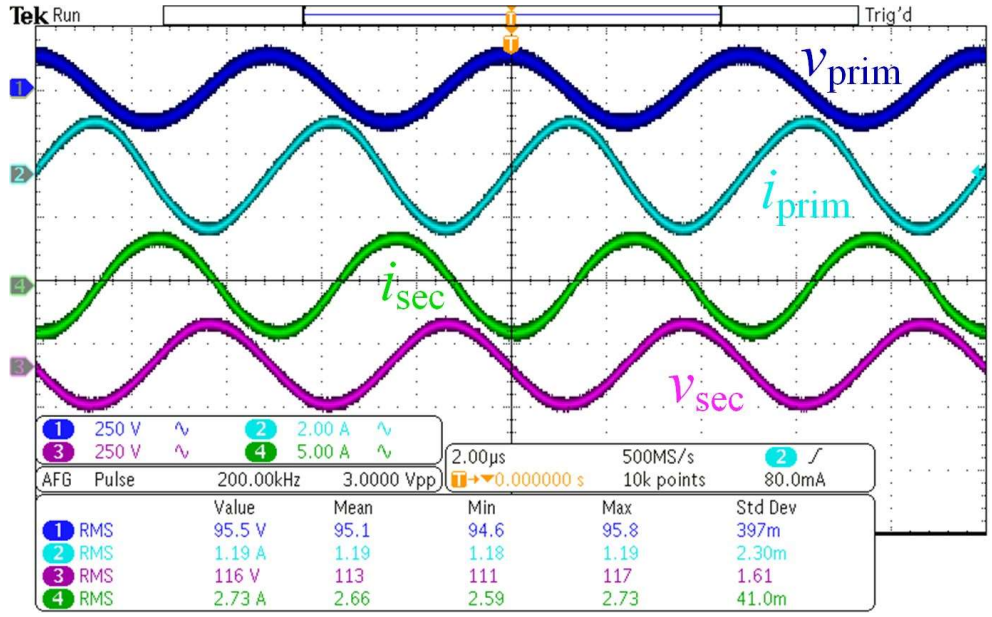

Fig. 5.27. Primary side voltage and current with secondary side voltage and current during WPT.

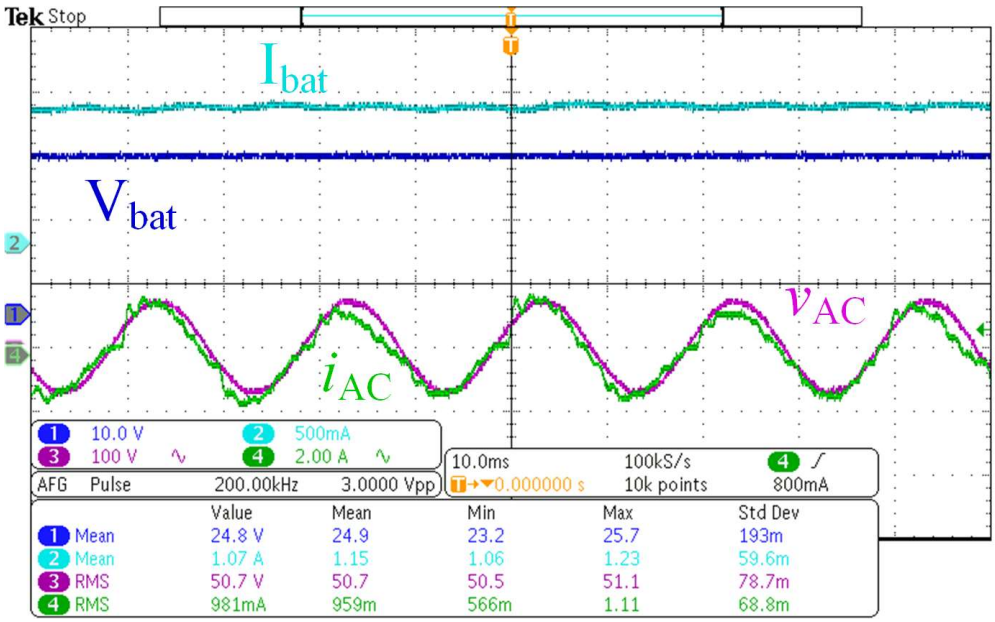

Fig. 5.28. Battery voltage and current with PFC operation at the input grid side during wireless charging.

During charging a 24 V, 30 Ah battery set; efficiency of the transmitting unit is 93.99%, the coil-to-coil efficiency is 92.49% and the rectification efficiency is 96.96%. The overall efficiency of the complete system during the wireless charging mode is found to be 85.92%.

5.5.3.2 Power Loss Analysis and Distribution

The loss calculation during the wireless charging mode is divided into three stages: 1) transmitting side converter 2) WPT system and 3) receiving side converter.

The detailed loss analysis and distribution is done only for the transmitting side converter as the losses in WPT unit only depends on the coil losses and its misalignment. Further, the losses in the receiving side converter is only contributed by the body diodes of the switches. The total loss in the transmitting side converter is found to be 13.6 W, while delivering power of 212.9 W at 93.99% efficiency. Considering the total losses of 13.6 W as 100%, percentage losses across different components are calculated and presented in Table 5.3. The same data is presented as bar chart in Fig. 5.29.

Table 5.3. Power Loss Distribution in various Components of RPP during Wireless Charging Mode

Devices	Conduction losses	Switching losses	Total losses	%age of total
S_A, S_B	1 W (7.3%)	2.5 W (18.3%)	3.5 W	25.6%
D_A, D_B	3 W (22%)	--	3 W	22%
S_{inv}	0.1 W (0.7%)	0 W	0.1 W	0.7%
L_{boost} (AC-DC)	--	--	1 W	7.3%
L_{in} (EF_2)	--	--	1 W	7.3%
Resonant inductors	--	--	3 W	22.5%
Capacitors all	--	--	2 W	14.6%

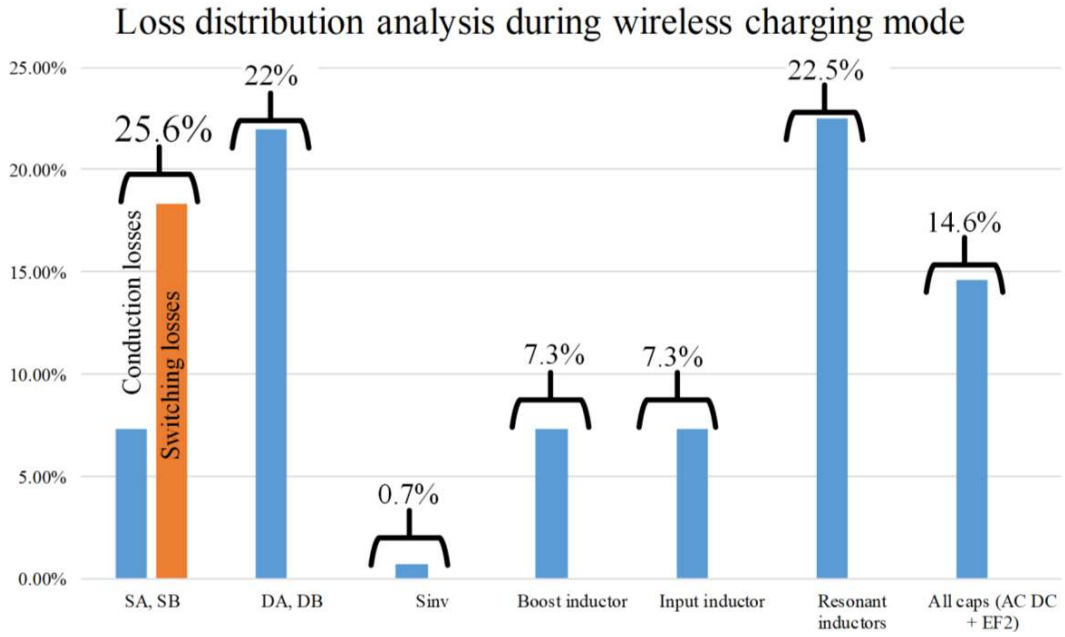

Fig. 5.29. Loss distribution across various components during wireless charging mode.

5.6 Merit Indices

5.6.1 Component Utilization Factor

The main idea behind the proposed concept is to reutilize the same components in different modes. So, the component utilization factor (CUF) plays a crucial role and becomes the most important performance parameter in deciding the adaptability of the reconfigurable power processor. The CUF is defined as the ratio of the numbers of components utilized in a particular mode to the actual number of components present in the package. Therefore, a power processor with higher CUF value is considered as a better choice as this uses more number components out of the available components in the package. The CUF in different modes for the proposed RPP are compared with various integrated chargers already reported in the literature and are given in Table 5.4. It is evident from the Table I that the proposed RPP has highest CUF as compared to its counterparts and moreover this is the only one, which can cater all three operations using a single power electronic package.

Table 5.4. CUF Comparison of the Proposed RPP with the Already Available Topologies

Sl. No.	References	No of switches used in			Total No. of switches in the package (T)	CUF		
		Wired-charging mode (X)	Wireless charging mode (Y)	Propulsion mode (Z)		Wired-charging mode (X/T)	Wireless charging mode (Y/T)	Propulsion mode (Z/T)
1	[65]	10	--	10	10	1	--	1
2	[67]	10	--	6	10	1	--	0.6
4	[96]	8	4	--	8	1	0.5	--
5	Proposed	8	4	6	8	1	0.5	0.75

5.6.2 Savings in Cost

The proposed schematics uses minimum number of components (semiconductor devices and passive elements) that leads to a more feasible solution from economic point of view. A cost break-up comparative analysis based on component counts is presented for three separate power processors in three different modes versus a single reconfigurable topology proposed in this work. The difference is calculated as percentage saving in both the cases and presented in

Table 5.5. The switch count in the conventional power processors are based on the number of switches in the corresponding topologies formed during different modes of the proposed RPP. This improvement in percentage saving is very high when compared with the conventional powertrain architectures available in the literature for motoring, wired charging and wireless charging systems.

Table 5.5. Percentage Saving in Implementing the Proposed RPP

Sl. No.	Components	Conventional Power Processor				Proposed RPP	Percentage Saving
		Wired Charger	Wireless charger	Propulsion unit	Total		
1.	Switching Devices	6	--	6	12	6	50 %
2.	Diodes	2	4	--	6	2	66.66 %
3.	Heat Sink	1	1	1	3	1	66.66 %
4.	Gate Driver and Accessories	6	--	6	12	6	50 %
5.	PCB Printing Cost	1	1	1	3	1	66.66 %
6.	Sensors	5	2	--	7	4	42.85 %
7.	Controller	1	--	1	2	1	50 %
9.	Contactors	----	---	----	----	5	Additional cost

5.7 Conclusion

A reconfigurable on-board power processor is presented in this chapter that serves as three different power converter topologies during three different modes: motoring, wired charging and wireless charging. A propulsion unit is considered as the backbone of the proposed RPP, which converts DC power to 3-phase AC for driving the motor. The proposed power processor restructures itself to three different converter topologies by changing the connection among the elements. This is achieved by using four point contactors, where the fixed contact of each contactors is connected to any one of the three positions to provide three modes of operations. The derived circuit, its mathematical analysis and the control scheme during all three modes are elaborated to give a clear picture of the proposed power processor. A test prototype of the proposed power processor is developed in the laboratory, and is satisfactorily tested in all three modes. The proposed schematic for transmitting side power converter is also developed and experimentally verified during wireless charging mode. The

complete experimental setup is tested using a 400 W BLDC motor and 24 V, 30 Ah battery set. The loss distribution and power loss analysis is also done for both the charging modes.